

Supersolid phase accompanied by a quantum critical point in the intermediate coupling regime of the Holstein model

Yuta Murakami,¹ Philipp Werner,² Naoto Tsuji,¹ and Hideo Aoki¹

¹*Department of Physics, University of Tokyo, Hongo, Tokyo 113-0033, Japan*

²*Department of Physics, University of Fribourg, 1700 Fribourg, Switzerland*

(Dated: February 27, 2014)

We reveal that the electron-phonon system as modeled by the Holstein model on a bipartite lattice exhibits, away from half filling, a supersolid (SS) phase characterized by coexisting charge order (CO) and superconductivity (SC), and an accompanying quantum critical point (QCP). The SS phase, demonstrated by the dynamical mean-field theory with a quantum Monte Carlo impurity solver, emerges around the peak of the T_c dome between the BCS and BEC regimes, while both in the weak- and strong-coupling regimes the CO/SC boundary is of first order with no intervening SS phases. The QCP is associated with the continuous transition from SS to SC with diverging charge fluctuations. We show that the SS/SC transition is hallmarked by a peaked kink in the superfluid density and that CO exhibits a reentrant behavior near the QCP.

PACS numbers: 71.38.-k, 71.10.Fd, 71.10.-w

Introduction— The competition between off-diagonal long-range order (ODLRO) and diagonal long-range order (DLRO) is an issue of central interest in various classes of strongly correlated systems [1–7]. An important question is whether ODLRO and DLRO can coexist and whether there exist associated quantum critical points (QCPs). Specifically, the phase may be called a supersolid state (SS) when a DLRO as a charge order (CO) and an ODLRO (superfluidity or superconductivity (SC)) coexist. SS phases have been investigated in bosonic systems, typically liquid helium [2], but also in boson-fermion mixtures [3] and spin systems [4]. In electron systems, related phenomena have been observed. For example, it has been recently found that a compound in the iron-based superconductor family, $\text{BaFe}_2(\text{As}_{1-x}\text{P}_x)_2$, exhibits a QCP accompanied by a non-Fermi liquid behavior, which separates SC and a phase in which SC and antiferromagnetism (AF) coexist [5]. For the cuprate superconductors, the possible existence of coexisting phases and QCP are intensively discussed in relation to the pseudogap [6, 7].

An important class of materials that provide an arena for competition between ODLRO and DLRO is a family of strongly-correlated electron-phonon systems with relatively large phonon energies and phonon-mediated attractive interactions comparable with the electronic bandwidth. A coexistence of s -wave SC and CO has been reported and discussed for $\text{Ba}(\text{Bi,Pb})\text{O}_3$ and $(\text{Ba,K})\text{BiO}_3$ [1]. The alkali-doped fullerenes [8] also accommodate the competition s -wave SC, AF. Although there are phenomenological arguments for explaining the coexistence of different phases [1, 9], a full understanding based on a microscopic model has yet to come.

In this paper, we focus on the Holstein model on a bipartite lattice away from half filling to address the question whether SS phases and QCPs exist in such a simplest possible model for electron-phonon systems, without ad-

ditional complexities (e.g., lattice frustrations or long-range interactions), and what their characteristic properties would be. There is in fact a long history for studies on strongly-coupled electron-phonon systems based on the Holstein(-Hubbard) model [10–18]. The model is known to favor CO at half filling, while a SC phase emerges away from half filling [10–15]. However, what happens around the boundary of CO and SC has not been fully investigated. Ref. [10] studied the model in one dimension and showed that there is a coexisting region of SC and CO in the sense of a quasi-ordered phase in 1D. In Ref. [15], ordered states are dealt with in the strong-coupling limit, but the possibility of phase separation has not been considered.

Here we employ, for a systematic investigation of the ordered phases in the Holstein model, the dynamical mean-field theory (DMFT) [19–21] with a continuous-time quantum Monte Carlo method (CTQMC, hybridization expansion) as an impurity solver [18, 22–24]. We shall show that a SS phase indeed emerges in the intermediate-coupling regime, where the peak of the T_c dome is located. The transition from SS to SC turns out to be continuous with diverging charge fluctuations, which suggests the presence of a QCP at $T = 0$. We also show that the phase transition is hallmarked by a peak in the superfluid density. Further, the charge order exhibits a peculiar reentrant behavior around the QCP. Curiously, the SS appears only in the intermediate coupling regime, which is consistent with weak- and strong-coupling perturbative calculations [25, 26].

Model — We consider the Holstein model,

$$H = -t \sum_{\langle i,j \rangle, \sigma} (c_{i\sigma}^\dagger c_{j\sigma} + \text{H.c.}) - \mu \sum_i (n_{i\uparrow} + n_{i\downarrow}) + g \sum_i (b_i^\dagger + b_i)(n_{i\uparrow} + n_{i\downarrow} - 1) + \omega_0 \sum_i b_i^\dagger b_i, \quad (1)$$

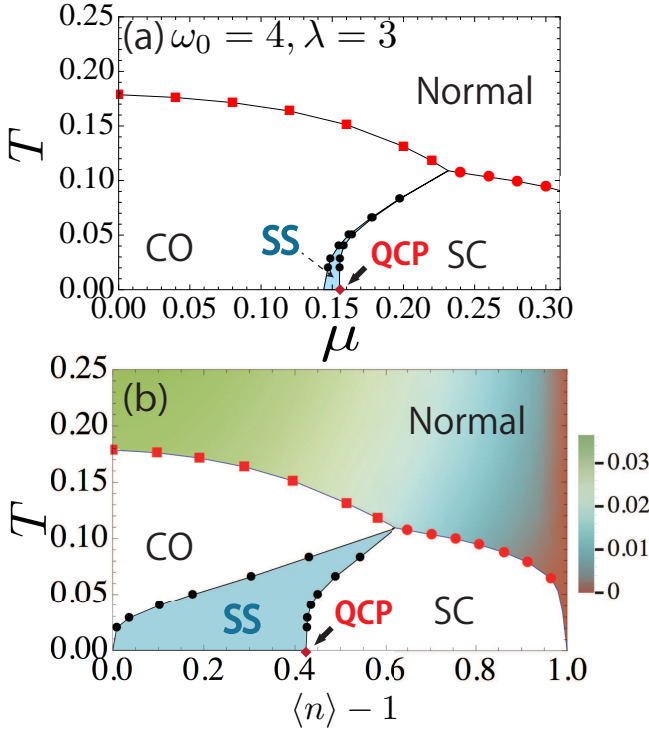


FIG. 1: (Color online) Phase diagram of the Holstein model plotted against (a) the chemical potential μ , and (b) the band filling n for $\omega_0 = 4$, $\lambda = 3$. Blue areas indicate the supersolid (SS) region, while red diamonds at $T = 0$ denote the quantum critical point (QCP). In the normal state, the dc conductivity is shown by color coding.

where i, j are site indices, $c_{i\sigma}^\dagger$ creates an electron at site i with spin σ , b_i^\dagger creates a phonon with frequency ω_0 at site i , t is the hopping parameter between nearest-neighbor sites, $n_{i\sigma}$ the number of electrons, μ the chemical potential, and g the electron-phonon coupling. The effective static phonon-mediated attractive interaction between electrons is $-\lambda \equiv -2g^2/\omega_0$.

Here, we focus on the regime where ω_0 is comparable to the electronic bandwidth W . This situation is realized in carbon based compounds such as alkali-doped fullerenes or the recently found aromatic superconductors [30]. In the DMFT calculation, we employ a Bethe lattice with infinite coordination, which has a semi-circular density of states, $\rho_0(\epsilon) = (4/\pi W)\sqrt{1 - (2\epsilon/W)^2}$ so that we use $W/4$ as the unit of energy. We consider s-wave SC and staggered CO as ordered phases. The order parameters are, respectively, $\Phi_{\text{SC}} = \frac{1}{N} \sum_i \langle c_{i\downarrow} c_{i\uparrow} \rangle$ and $\Phi_{\text{CO}} = |n_A - n_B|/4$, where N is the total number of lattice sites, and A and B denote sublattices. The phase boundaries are identified by the onsets of these order parameters. Green's functions are collected on a grid of $N_\tau = 4 \cdot 10^3$ points in the DMFT+CT-QMC calculations.

Results— The main result of our paper is the DMFT+CT-QMC phase diagram away from half filling,

displayed in Fig. 1 for $\lambda = 3$ with $\omega_0 = 4$. Panel (a) plots the phase boundaries as a function of the chemical potential μ and panel (b) as a function of the electronic filling n . Notably, we find, in both panels, a SS region between SC and CO in which the order parameters Φ_{SC} (an ODLRO) and Φ_{CO} (DLRO) are both nonzero. Since this SS phase appears in a finite region even on the μ axis, it should be robust against external fields or phase separation into SC and CO. We have confirmed the existence of the SS phase for smaller values of ω_0 such as $\omega_0 = 2$. The phase boundaries between SS/SC and SS/CO are of second order as discussed below. In both of μ - T and n - T phase diagrams, the SS region widens as temperature decreases. For $T \rightarrow 0$, the SS phase appears at a nonzero value of μ (≈ 0.145), which corresponds to $\langle n \rangle = 1$ (half filling), so that the SS phase appears upon small doping from half filling. The continuous transition between SS and SC at finite temperatures suggests that this boundary ends at a QCP at $T = 0$. We also note that the SS region is located below the CO phase (see Fig. 1(a)(b)), and that in the filling range $0.43 < \langle n \rangle - 1 < 0.6$, the CO order Φ_{CO} emerges and then disappears as temperature decreases. This behavior is qualitatively different from the phase diagram of $\text{BaFe}_2(\text{As}_{1-x}\text{P}_x)_2$ [5], where the SC+AF phase appears below both SC and AF.

To have a closer look at the behavior near the SC/CO boundary, we plot the order parameters in Fig. 2 against μ (panel (a)) and against $\langle n \rangle$ (panel (b)), along with $\langle n \rangle$ vs μ (panel (c)) for $\lambda = 3, \omega_0 = 4$, and the inverse temperature $\beta = 35$. In the SS phase between SC and CO ($0.149 \lesssim \mu \lesssim 0.156$), both Φ_{SC} and Φ_{CO} are indeed nonzero. Panel (c) indicates that the compressibility, $\partial n / \partial \mu$ is highly enhanced in the SS. More importantly, SS and SC are not only continuously connected, but the static charge susceptibility $\chi_{\mathbf{Q}}$ at $\mathbf{Q} = (\pi, \pi)$, whose inverse is plotted in Fig. 2(d), diverges like $1/(n - n_c)$ at the critical value n_c that corresponds to the SC/SS boundary. This divergence confirms the second-order nature of the phase transition. Here the susceptibility is computed by applying a small staggered external field $H_{\text{ext}} = \delta\mu(N_A - N_B)$, where $N_{A,B} = \sum_{i \in A,B} n_i$, with $\delta\mu = 2 \times 10^{-4}$ for SS and $\delta\mu = 5 \times 10^{-4}$ for SC. Another interesting quantity is the London penetration depth λ_L , because the superfluid density is proportional to $\lambda_L^{-2} = -(c^2/4\pi N)[\chi_{J,J}(i0^+) - e^2 \sum_{\mathbf{k},\sigma} \langle (\partial^2 \epsilon(\mathbf{k}) / \partial k_x^2) c_{\mathbf{k},\sigma}^\dagger c_{\mathbf{k},\sigma} \rangle]$. Here $\chi_{J,J}(\nu)$ is the current-current correlation function, c the speed of light, e the elementary charge and the lattice constant set to be unity. The general form of $\chi_{J,J}(i\nu_n)$ applicable to SC, SS and CO is given in the supplement. The behavior of λ_L^{-2} in the SC and SS phases is shown in Fig. 2(d). We find that the boundary of SC and SS exhibits a kink (maximum) in λ_L^{-2} . This means that, in SC, the superfluid density increases toward the half filling ($n - 1 = 0$) because the DOS of the free system increases favoring SC, while in SS, CO component increasing to

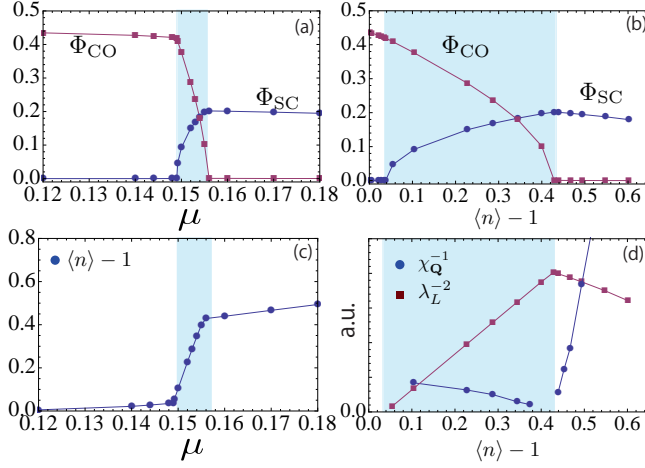


FIG. 2: (Color online) SC and CO order parameters against μ (a), or against n (b). (c) The evolution of the density as a function of μ . Blue areas indicate the region of SS. (d) Inverse of the static charge susceptibility, $\chi_{\mathbf{Q}}$ at $\mathbf{Q} = (\pi, \pi)$, and the inverse of the squared London penetration depth λ , against the density. The parameters are $\omega_0 = 4, \lambda = 3, \beta = 35$.

ward half filling weakens SC.

At the boundary between CO and SS, the order parameters also appear to be continuously connected, see Fig. 2. This suggests that the boundary between CO and SS is of second order as well. While the CO solution can be extended to larger fillings by suppressing SC, this solution becomes unstable against an introduction of a small SC component in the SS region. That the SS is more stable than CO can be understood as follows. The free energy is $\Omega(T, \mu) = -T \ln[\text{Tr} \exp(-\beta H)]$ and $N^{-1} \partial \Omega(T, \mu) / \partial \mu = -\langle n \rangle$. Since the SS and CO solutions are continuously connected at the critical μ , and the SS solution has a larger filling than the CO solution for a given μ (Fig. 2(c)), it follows that the SS is lower in free energy.

Now we display the phase diagram against the phonon-induced attractive interaction λ and chemical potential μ in Fig. 3(a) for $\omega_0 = 4, \beta = 35$. The SS region is widest around $\lambda = 3$, while we find no SS phase for $\lambda = 2$ nor for $\lambda = 4.5$. We argue that the SS phase and associated QCP emerge only in the intermediate-coupling regime characterized by the peak of the T_c dome (which roughly corresponds to the BCS-BEC crossover region[34]). In fact, if we look at the λ -dependence of the transition temperatures for SC and CO at half filling (Fig. 3(b)), we find the peaks of the T_c domes are located around $\lambda \simeq 3$ for both of SC and CO at $\omega_0 = 4$. We also plot the transition temperatures as a function of filling in Fig. 3(c). We can see that $\lambda = 3$ has indeed the highest transition temperature at $\omega_0 = 4$, independent of filling. At this intermediate coupling ($\lambda \sim 3$), a metal-insulator crossover occurs in the normal phase as one changes λ . At $\lambda = 3$, we observe

that the dc conductivity ($\text{Re}\sigma(0)$) increases with increasing temperature, as indicative of an insulating behavior, in the whole range of the doping [Fig. 1(b)]. On the other hand, the metallic behavior shows up at $\lambda = 2.5$ for all doping (not shown). An insulating behavior at $\lambda = 3$ is also evident in the spectral functions derived from the Maximum entropy method in Fig. 3(d), which exhibits a pseudogap-like structure with a dip between the well developed bands in the density of states around $\omega = 0$. We note that the correlation among the SS region, the peak of T_c dome and the metal-insulator crossover point holds even for lower ω_0 such as $\omega_0 = 2$, where all of them moves to smaller λ .

The absence of the SS phase in the weak- ($\lambda \leq 2$) and strong-coupling ($\lambda \geq 4$) regimes is consistent with perturbation theories. In the weak-coupling regime, we employ the second-order weak-coupling expansion as an impurity solver for DMFT (IPT), where we expand all the self-energy diagrams including the Hartree term up to second order in λ [29]. While the normal state of the Holstein model has been studied with DMFT in combination with weak-coupling approximations for the impurity solver[13, 14], here we extend this to the ordered phases. Figure 4(a) displays the IPT phase diagram and the variation of $\langle n \rangle$ with μ . We find that, between SC and CO, there is a first order transition with a hysteretic region (shaded in Fig. 4(a)), where CO and SC are respectively stable DMFT solutions. The hysteretic region for the two solutions has been determined as follows. For SC, we use the local Green's function for μ as an initial input for $\mu - \delta\mu$ ($\delta\mu = 0.001$ here). For CO, we first derive a CO solution by suppressing SC, and then add a small

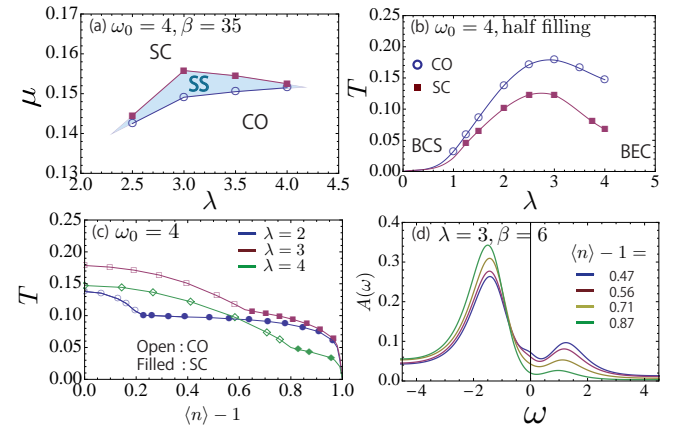


FIG. 3: (Color online) (a) A $\lambda - \mu$ phase diagram (μ : chemical potential, λ : strength of the interaction) in the SS region for $\omega_0 = 4, \beta = 35$. (b) Transition temperatures for CO and SC against λ at half filling for $\omega_0 = 4$. CO is suppressed to obtain the T_c for SC. (c) Transition temperatures for CO and SC against the filling at $\omega_0 = 4$ without any restriction on the orders. (d) Spectral functions in the normal state at $\omega_0 = 4, \lambda = 3, \beta = 6$.

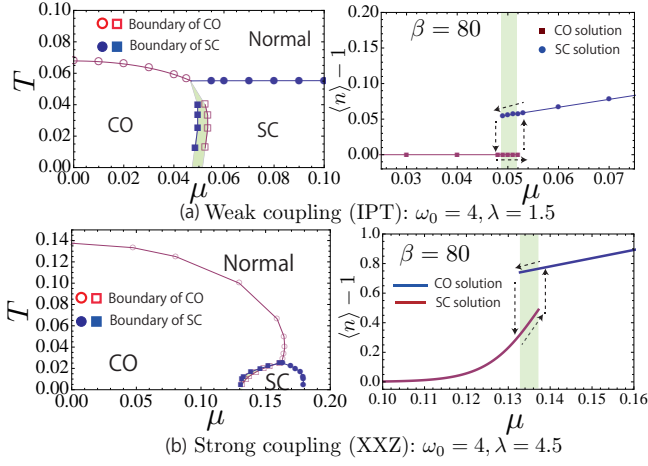


FIG. 4: (Color online) (a) Results of IPT + DMFT at $\omega_0 = 4, \lambda = 1.5$. Left panel shows the phase diagram, while the right one plots $\langle n \rangle - 1$ against μ at $\beta = 80$. (b) Results of the mean-field analysis for the effective spin model, Eq. (2), at $\omega_0 = 4, \lambda = 4.5$. Left panel is the phase diagram, while the right one plots $\langle n \rangle - 1$ as a function of μ at $\beta = 80$. Green areas indicate hysteretic region for CO and SC.

anomalous part ($\Phi_{SC} \sim 0.002$) to see whether it grows or vanishes. In these IPT calculations, we have found no stable self-consistent SS solution, but it always converges to either SC or CO. We have checked that the same conclusion holds for even smaller interactions (e.g., $\lambda = 1$) and is confirmed by other perturbative approximations such as the conserving Hartree-Fock approximation [13] and the second-order conserving approximations [14].

On the other hand, if one performs a $1/\lambda$ expansion around the strong-coupling limit ($\lambda \rightarrow \infty$), the leading-order effective model becomes an XXZ model with nearest-neighbor exchange coupling [25, 26],

$$H_{\text{eff}} = -2\mu \sum_i (S_i^z + 1/2) - J_1 \sum_{\langle i,j \rangle} (S_i^x S_j^x + S_i^y S_j^y) + J_2 \sum_{\langle i,j \rangle} (S_i^z S_j^z - 1/4). \quad (2)$$

Here, J_1 and J_2 are functions of g and ω_0 . In the limit of infinite spatial dimensions ($d \rightarrow \infty$), J_1 and J_2 scale as $1/d$ and the mean-field solution of the effective spin system becomes exact. The result of the mean-field analysis is shown in Fig. 4 (b), where we have numerically solved the self-consistency equation. At $T = 0$, the result is consistent with Ref. [28]: there is no finite SS region if one plots the phase diagram against μ (an external field in the spin model). Precisely at $\mu = (zJ_2/2)\sqrt{1 - (J_1/J_2)^2}$, where z is the coordination number, the SC, CO and SS phases become all degenerate. While this may seem to indicate a SS region if one plots the phase diagram against n [15, 27], this occurs only at a single point on the μ -axis,

so that the SS is expected to be fragile against external perturbations and/or against phase separation into SC and CO. At non-zero temperature, there is a tiny but finite hysteretic region where the solutions converge to either SC or CO [Fig. 4(b)] with no intervening stable SS solutions. We have checked this by adding small perturbations to the self-consistent solutions. We thus conclude that neither the weak-coupling nor the strong-coupling approximations predict a SS phase in the corresponding regimes.

Since, near the optimum region ($\lambda = 3$) for the SS, the normal state shows an insulating behavior, we can discuss the stability of the SS phase in the strong-coupling framework. It is known that the higher-order terms in the strong-coupling expansion lead to longer-range exchange interactions as well as four spin terms in the effective spin model [26]. While the details should depend on the value of the parameters, it is known that longer-ranged exchange interactions can favor SS [28], which provides an explanation for the appearance of the SS solution in the intermediate coupling regime.

Conclusion – We have investigated the ordered phases in the Holstein model in bipartite (i.e., non-frustrated) lattices away from half filling with DMFT+CT-QMC. We have focused on the unconventional region where λ and ω_0 are comparable to the bandwidth W . Our study revealed the existence of a supersolid phase in the intermediate-coupling regime. The phase diagram contains a QCP which separates the SS and SC phases. The SS phase is located entirely below the CO phase, and the phase transition from SC and SS is characterized by a downward (upward) kink in the London penetration depth (superfluid density). The absence of a stable SS phase in the weak- and strong-coupling regimes has been confirmed by perturbative analyses. Our results suggest that phenomena related to the SS phase and associated QCP may be explored in carbon-based compounds, some of which belong to the unconventional parameter regime considered here. Further comparison with the related problem of AF+SC should help to understand the competition and coexistence of DLRO and ODLRO.

Acknowledgements. We thank D. Yamamoto and S. Yamazaki for helpful discussions. The simulations have been performed with a code based on ALPS [31]. YM, NT and HA have been supported by LEM-SUPER (EU-Japan Superconductor Project) from JST, while PW acknowledges support from SNF Grant 200021-140648 and FP7/ERC starting grant No. 278023.

-
- [1] A. M. Gabovich et al, Phys. Rep. **367**, 583 (2002).
 - [2] E. Kim and M. H. W. Chan, Nature (London) **427**, 225 (2004); E. Kim and M. H. W. Chan, Phys. Rev. Lett

- 109**, 155301 (2012); P. Sengupta, L. P. Pryadko, F. Alet, M. Troyer, and G. Schmid, Phys. Rev. Lett. **94**, 207202 (2005); D. Yamamoto, I. Danshita, and C. A. R. Sá de Melo, Phys. Rev. A **85**, 021601(R) (2012).
- [3] P. Anders, P. Werner, M. Troyer, M. Sigrist, and L. Pollet, Phys. Rev. Lett. **109**, 206401 (2012).
- [4] K. K. Ng and T. K. Lee, Phys. Rev. Lett. **97**, 127204 (2006); P. Sengupta and C. D. Batista, Phys. Rev. Lett. **98**, 227201 (2007); N. Laflorencie and F. Mila, Phys. Rev. Lett. **99**, 027202 (2007); D. Yamamoto and I. Danshita, Phys. Rev. B **88**, 014419 (2013); Y. Murakami, T. Oka and H. Aoki, Phys. Rev. B **88**, 224404 (2013).
- [5] K. Hashimoto *et al*, Science **336**, 1554 (2012).
- [6] G. Ghiringhelli *et al*, Science **337**, 821 (2012).
- [7] W. D. Wise *et al*, Nat. Phys. **4**, 696 (2008).
- [8] Y. Takabayashi *et al*, Science **323**, 1585 (2009); M. Capone *et al*, Rev. Mod. Phys. **81**, 943 (2009); O. Gunnarsson, Rev. Mod. Phys. **69**, 575 (1997).
- [9] G. Bilbro and W. L. McMillan, Phys. Rev. B **14** 1887 (1976).
- [10] M. Tezuka, R. Arita, and H. Aoki, Phys. Rev. Lett. **95**, 226401 (2005); Phys. Rev. B **76**, 155114 (2007).
- [11] R.T. Scalettar, N.E. Bickers, and D.J. Scalapino, Phys. Rev. B **40**, 197 (1989).
- [12] R.M. Noack, D.J. Scalapino, and R.T. Scalettar, Phys. Rev. Lett. **66**, 778 (1991).
- [13] J. K. Freericks, M. Jarrell, and D. J. Scalapino, Phys. Rev. B **48**, 6302 (1993).
- [14] J. K. Freericks and M. Jarrell, Phys. Rev. B **50**, 6939 (1994); J. K. Freericks, Phys. Rev. B **50**, 403 (1994).
- [15] A. S. Alexandrov, J. Ranninger, and S. Robaszkiewicz, Phys. Rev. B **33**, 4526 (1986).
- [16] E. A. Nowadnick, S. Johnston, B. Moritz, R. T. Scalettar, and T. P. Devereaux, Phys. Rev. Lett. **109**, 246404 (2012).
- [17] J. Bauer, EPL **90**, 27002 (2010); J. Bauer and A. C. Hewson, Phys. Rev. B **81**, 235113 (2010).
- [18] Y. Murakami, P. Werner, N. Tsuji and H. Aoki, Phys. Rev. B **88**, 125126 (2013).
- [19] W. Metzner and D. Vollhardt, Phys. Rev. Lett. **62**, 324 (1989).
- [20] A. Georges and G. Kotliar, Phys. Rev. B **45**, 6479 (1992).
- [21] A. Georges, G. Kotliar, W. Krauth, and M. J. Rozenberg, Rev. Mod. Phys. **68**, 13 (1996).
- [22] P. Werner and A. J. Millis, Phys. Rev. Lett. **99**, 146404 (2007).
- [23] P. Werner, A. Comanac, L. de'Medici, M. Troyer, and A. J. Millis, Phys. Rev. Lett. **97**, 076405 (2006).
- [24] E. Gull, A. J. Millis, A. I. Lichtenstein, A. N. Rubtsov, M. Troyer, and P. Werner, Rev. Mod. Phys. **83**, 349 (2011).
- [25] J. E. Hirsch and E. Fradkin, Phys. Rev. B **27**, 4302 (1983).
- [26] J.K. Freericks, Phys. Rev. B **48**, 3881 (1993).
- [27] S. Robaszkiewicz, R. Micnas, K. A. Chao, Phys. Rev. B **23**, 1447 (1981).
- [28] H. Matsuda and T. Tsuneto, Suppl. Prog. Theor. Phys. **46**, 411 (1970).
- [29] N. Tsuji and P. Werner, Phys. Rev. B **88**, 165115 (2013).
- [30] T. Kato, T. Kambe, and Y. Kubozono, Phys. Rev. Lett. **107**, 077001 (2011); Y. Kubozono *et al*, Phys. Chem. Chem. Phys. **13**, 16476 (2011); T. Kosugi *et al*, Phys. Rev. B **84**, 214506 (2011); A. Subedi and L. Boeri, Phys. Rev. B **84**, 020508(R) (2011); Y. Nomura, K. Nakamura, and R. Arita, Phys. Rev. B **85**, 155452 (2012).
- [31] A. Albuquerque *et al*, J. Magn. Magn. Mater. **310**, 1187 (2007); B. Bauer *et al*, J. Stat. Mech.: Theor. Exper. (**2011**) P05001.
- [32] L.-F. Arsenault and A. M. S. Tremblay, Phys. Rev. B **88**, 205109 (2013).
- [33] A. Toschi, M. Capone, and C. Castellani, Phys. Rev. B **72**, 235118 (2005).
- [34] We note that, strictly speaking, the peak of T_c dome does not necessarily coincide with the BCS-BEC crossover point, as is suggested for the attractive Hubbard model[33].

Supplementary material

Here we show the general expression for the current-current correlation function applicable to normal, CO, SC and SS states. To investigate transport properties on the Bethe lattice, the formulas are adapted from those for a d -dimensional hypercubic lattice, by substituting a semi-circular density of states [32]. We can adopt the x -component without loss of generality, i.e. χ_{J_x, J_x} . Within DMFT, the vertex correction disappears because of the parity symmetry, and we can express the correlation function in terms of Green's functions alone,

$$\begin{aligned} \chi_{J_x, J_x}(i\nu_n) = & -\frac{e^2}{\beta} \sum_{\omega_n, \alpha, \alpha'} \int d\epsilon \Phi_{x,x}(\epsilon) \left[G_{\mathbf{0}}^{\alpha', \alpha}(\epsilon, i\omega_{n_1}) G_{\mathbf{0}}^{\alpha, \alpha'}(\epsilon, i\omega_n + i\nu_n) \right. \\ & \left. - G_{\mathbf{Q}}^{\alpha', \alpha}(\epsilon, i\omega_n) G_{\mathbf{Q}}^{\alpha, \alpha'}(-\epsilon, i\omega_n + i\nu_n) \right]. \end{aligned} \quad (3)$$

Here, $\epsilon_{\mathbf{k}}$ is the energy of free electrons with momentum \mathbf{k} , $\Phi_{x,x}(\epsilon) \equiv \sum_{\mathbf{k}} (\partial \epsilon_{\mathbf{k}} / \partial k_x)^2 \delta(\epsilon - \epsilon_{\mathbf{k}})$, $G_{\mathbf{q}}^{\alpha, \alpha'}(\epsilon_{\mathbf{k}}, i\omega_n) = -\int_0^\beta \langle T_\tau c_{\mathbf{k}, \alpha}(\tau) c_{\mathbf{k}+\mathbf{q}, \alpha'}^\dagger(0) \rangle e^{i\omega_n \tau}$ with $\mathbf{q} = \mathbf{0}$ or \mathbf{Q} , $\alpha, \alpha' = 1, 2$, $c_{\mathbf{k}, 1} = c_{\mathbf{k}, \uparrow}$, and $c_{\mathbf{k}, 2} = c_{-\mathbf{k}, \downarrow}^\dagger$. For the Bethe lattice $\Phi_{x,x}(\epsilon) = (N/3d)[(W/2)^2 - \epsilon^2]\rho_0(\epsilon)$ [32], where N is the size of system and $2d$ the coordination number. Furthermore, we use $\sum_{\mathbf{k}} (\partial^2 \epsilon_{\mathbf{k}} / \partial k_x^2) \delta(\epsilon - \epsilon_{\mathbf{k}}) = d\Phi_{x,x}(\epsilon)/d\epsilon$ to evaluate $e^2 \sum_{\mathbf{k}, \sigma} \langle (\partial^2 \epsilon(\mathbf{k}) / \partial k_x^2) c_{\mathbf{k}, \sigma}^\dagger c_{\mathbf{k}, \sigma} \rangle$ [32]. We also note that the above expression at $\nu_n = 0$ corresponds to $\chi_{J_x, J_x}(i0^+)$ if the system is correlated. Since, in normal states, the dc conductivity is expressed as $\text{Re}\sigma(0) = -\lim_{\nu \rightarrow 0^+} [\chi_{J_x, J_x}(i\nu) - \chi_{J_x, J_x}(i0^+)]/\nu$, we interpolate $\chi_{J_x, J_x}(i\nu_n)$ for $n = 0, 1, \dots$ with polynomials of second or third order or the Pade approximation to evaluate $\text{Re}\sigma(0)$. In Fig. 1, we have shown the results for the second-order interpolation, but we note that all of these interpolations give qualitatively the same results.